Journal of Applied Polymer Science

WILEY

Applied Polymer SCIENCE

RESEARCH ARTICLE OPEN ACCESS

Multi-Material 3D Printing of Soft Dielectric Actuators With Optimized Electrodes

Ivan Raguž[1,2] | Michael Berer[1] | Clemens Holzer[2] | Bram Vanderborght[3] | Joost Brancart[4] | Sandra Schlögl[1,2]

[1]Polymer Competence Center Leoben GmbH, Leoben, Austria | [2]Department of Polymer Engineering and Science, Montanuniversitaet Leoben, Leoben, Austria | [3]Brubotics, Vrije Universiteit Brussel and Imec, Brussels, Belgium | [4]Physical Chemistry and Polymer Science, Sustainable Materials Engineering, Vrije Universiteit Brussel, Brussels, Belgium

Correspondence: Sandra Schlögl (sandra.schloegl@unileoben.ac.at; sandra.schloegl@pccl.at)

Received: 28 May 2025 | **Revised:** 28 August 2025 | **Accepted:** 17 September 2025

Funding: This work was supported by Fonds Wetenschappelijk Onderzoek (12W4719N), Österreichische Forschungsförderungsgesellschaft (21647048, 904927).

Keywords: dielectric elastomer actuators | electrode | fused filament fabrication | multi-material 3D printing | soft active devices

ABSTRACT

Dielectric elastomer actuators (DEA) have gained increased attention in the design of electrically driven soft and lightweight robotic devices. They rely on Coulomb forces for their actuation and are able to undergo large displacements as a function of the applied electrical field. Fabricating DEAs with additive manufacturing opens the way to a personalized and cost-efficient fabrication of soft active devices. In particular, extrusion-based techniques provide a versatile strategy to multi-material 3D print DEAs by using electrically conductive and soft filaments with high elongation. One key aspect of DEAs is the electrode's performance, which has to provide a high electrical conductivity and a good adhesion to the sandwiched membrane. Herein, selected 3D printing parameters were varied to optimize the electrode infill density and electrode infill direction. Mechanical and electrical properties, as well as actuation performance, of fully 3D-printed DEA demonstrators were studied comprehensively. With the optimized parameter set, a maximum DEA displacement of 91% was achieved with respect to the free length of the actuator. This is comparable to the performance of non-3D-printed DEAs and demonstrates the potential of 3D printing for the production of DEAs undergoing large deformations while leveraging the design and manufacturing freedom of multi-material 3D printing.

1 | Introduction

Adaptable and multi-functional soft actuators are highly versatile and can be used for numerous applications ranging from interactions with humans [1, 2] to space explorations [3, 4]. Dielectric elastomer actuators (DEA) are an interesting type of soft actuators that convert an electrical stimulus into a mechanical displacement [5]. Although large electric fields have to be applied (typically around 100 V/μm), the DEA's mechanical response can be varied over several orders of magnitude of strain (from 10% to 300%) [6]. DEAs further provide the possibility to be prepared by cost-efficient and easily scalable processes, and they are lightweight, mechanically robust, and benefit from low cycling hysteresis [7].

Their working principle is mainly related to Coulomb forces that arise between the electrodes when a potential difference is applied across the opposite membrane sides [8]. The basic functional component of a DEA, the active component, consists of a flexible dielectric membrane being sandwiched between two flexible electrodes [9]. By combining the active component with a passive component or other geometric features, distinct DEA configurations

can be created, including stacked actuators, extenders, unimorph bending beam actuators, diaphragms, or tubes [10].

For the design of DEAs, elastomers with a high dielectric permittivity and a high dielectric breakdown voltage are used as membrane [6]. Depending on the type of elastomer, the electro-mechanical response can be either a result of the Maxwell stress effect (caused by the change in the electric field distribution within the dielectric membrane) or electrostriction. Electrostriction is the predominant mechanism in PVDF and liquid crystal elastomers, while silicone rubbers are mainly governed by Maxwell stress [11, 12]. In contrast, in thermoplastic elastomers and polyurethanes, both mechanisms contribute to the activation of the DEA [13].

The electrode should be characterized by a high electrical conductivity to ensure (fast) electrical charging and discharging of the actuator [7, 14–17]. With respect to an unhindered and reversible deformation of the actuator, both membrane and electrode should be soft (high mechanical compliance) and flexible (high and reversible deformability) [18–22]. Pelrine et al. stated that the ideal electrode should also be thin relative to the polymer thickness (to ensure that it does not compromise on the DEA's material performance) and patternable for its spatially controlled deposition [23]. Compliant electrodes are typically prepared using liquid polymers [24], hydrogels [25], highly filled polymer inks, or polymer nanocomposites [26]. Depending on the type of electrode material, various processing routes are pursued to fabricate (stacked) dielectric actuators. Li and coworkers cast and cured the electrode material [27] while Kelley et al. used a folding method in which silicon rubber sheets were folded into a stacked configuration and carbon powder as an electrode was applied manually [28].

Among the reported preparation techniques, 3D printing offers the advantage of a freedom in design in all three directions and provides a step change in fabrication speed. However, in most of the reported systems, the membrane is 3D printed while the electrode is applied separately in a post-processing step. For example, Rossiter and co-workers ink-jet 3D printed the dielectric layer for an antagonistic annular DEA and applied the electrodes manually by brushing a silver paste on [29]. The same group also reported on the fused filament fabrication (FFF) 3D printing of active membranes and support structures, and prepared DEAs by pressing together two printed actuator halves [29].

In FFF 3D printing, a subgroup of material extrusion (MEX), filaments of a thermoplastic polymer are deposited on the build platform, and the object is printed layer by layer by solidification of the polymer melt [30]. The printing method benefits from an ease of operation, availability of cost-efficient printers, a variety of (filled) filaments, and the possibility to multi-material 3D print structures by using printers with multiple extrusion heads [31]. Multi-material FFF enables a high design and manufacturing freedom that is unparalleled by any traditional manufacturing technique. This includes the controlled manufacturing of non-isotropic parts [32–34], which is advantageous for the fabrication of personalized DEAs [35].

In an elegant approach, Palmić and Slavič printed both membrane and electrode via multi-material FFF printing [36]. Along with the poor surface quality of FFF printed objects, they reported that the main challenge is the reliability and repeatability of the material deposition, which negatively affects the DEAs' performance. They also provided strategies to overcome common extrusion-based printing issues such as variations in layer thickness, porosity, and high surface roughness by rigorous control of the printing process and advanced inspection systems.

In a previous study, we multi-material FFF 3D-printed DEAs in a single printing job and optimized the dielectric membrane [16]. In contrast, the properties of the electrode were less explored, and it was fabricated by 3D printing a full layer of an electrically conductive filament (Eel TPU 3D) in two different printing directions (0° and 90°). In general, mechanical reinforcement and undesired stiffening of the DEA were observed by the additional 3D printing of the electrode material.

The current follow-up study aims to optimize the processing and geometry of the electrode to find a good balance between high electrical conductivity and low contribution to the DEA's bending stiffness. The latter aspect ensures that the actuator is able to undergo larger deformations and thus provides a better performance capability. A particular focus was put on the electrode infill density and electrode infill direction. Their influence on mechanical and electrical properties as well as actuation performance of fully 3D-printed DEA demonstrators was studied comprehensively, and structure–property relationships were established.

2 | Experimental Part

2.1 | Materials

For the printing of the dielectric membrane, NinjaFlex TPU (Fenner Inc., Manheim, USA) with a hardness of 85 Shore A was applied [37]. The filament for printing the electrode material was Eel TPU 3D (Fenner Inc., Manheim, USA) with a hardness of 90 Shore A [38]. The filaments were used as received.

2.2 | 3D Printing of DEAs

FFF printing was conducted with the dual-extruder FFF 3D printer "CreatBot F430" (Henan Suwei Electronic Technology Co. LTD., Zhengzhou City, Henan Province, China). The slicing software used was "Ultimaker Cura 4.6.2" (Ultimaker B.V., ED Utrecht, Netherlands). If not stated otherwise, the FFF processing parameters shown in Table S1 were applied. The general printing parameters and the printing parameters of the extruders were optimized in previous work [16].

2.3 | Quantifying the DEA Displacement

The electric voltage required for the actuation of the fully 3D printed DEA was achieved with the high voltage power supply "PHYWE 0–10 kV" (PHYWE Systeme GmbH und Co. KG, Göttingen, Germany). Figure S1 shows a schematic of the DEA experimental setup used to characterize the actuator's endpoint movement, from which the DEA performance in terms of

maximum displacement was determined. The fully 3D printed DEA was clamped in a home-built measurement holder. The DEA movement was monitored by an HD camera, and the image was processed by the data acquisition PC.

2.4 | Basic Electric Field Distribution Simulation

An electric simulation inspired by References [39, 40]. was conducted to provide insights into the electric field distribution within the dielectric membrane. For this, the simulation software "Ansys Workbench 2022 R2" (ANSYS Inc., 2600 Ansys Drive Canonsburg, PA 15317 US) was used. The simulation was performed based on the geometrical properties of the 3D printed DEAs with varying electrode infill densities (20%, 27%, 40%, 60%). A simplified dielectric membrane geometry (5.58 ×1 ×0.15 mm) (Figure S2) with defined electrode surfaces was modeled. A thickness of 0.15 mm was applied to mimic the thickness of the dielectric membrane of the 3D printed DEA. The geometry was meshed with cube finite elements of 0.01 mm side length. In total, the mesh had 837,000 finite elements. The actuation voltage applied to the electrode surfaces was 5 kV.

2.5 | Material Characterization

To experimentally simulate the stretching of the electrode upon actuation (and thus bending deformation) of the DEA, tensile tests were conducted using a Zwick/Roell Z1.0 tensile testing machine (Zwick GmbH & Co. KG., Ulm, Germany). For this, 3D-printed tensile films with a rectangular shape (120×45 mm) were used. The films consisted of two 0.1 mm thick layers. The first layer was a non-conductive layer 3D printed from the DEA membrane material (NinjaFlex TPU), and the second layer was a conductive layer, which simulated an electrode layer (Eel TPU 3D). For the electrode layer, the infill direction with respect to the specimen's longitudinal axis and the infill density were varied between 0° and 90°, and 20%–100%, respectively. An infill density of 20% yielded a distance of 1.6 mm between two adjacent electrode lines. For the other infill densities, these distances were as follows: 1.1 mm, 0.6 mm, 0.27 mm. An electrode infill density of 100% resulted in the fully printed electrode with 0 mm distance between the adjacent electrode lines. Figure 1a–c exemplarily show 3 tensile films (120×45 mm) printed with the same electrode infill density of 40% but with varying electrode infill directions (90°, 45°, and 0°). A total of three specimens per configuration were printed.

The tensile films were uniaxially stretched in a stress–electrical resistance–strain measurement set-up (Figure 1d) using the tensile testing machine. The testing speed was set to 30 mm/min and a preload force of 0.1 N was applied. Since the electrical resistance of the electrode was measured during the test, the use of plastic, electrically non-conductive clamping jaws was necessary to avoid any electric connection through the tensile testing machine. Copper strips, glued onto the plastic clamping jaws, were used as connectors for the electrical resistance measuring device, thereby also defining the clamping length of 60 mm. The position of these copper strips with respect to the specimen is illustrated in Figure 1d. The change in electrical resistance was measured with increasing strain using a "QuantumX

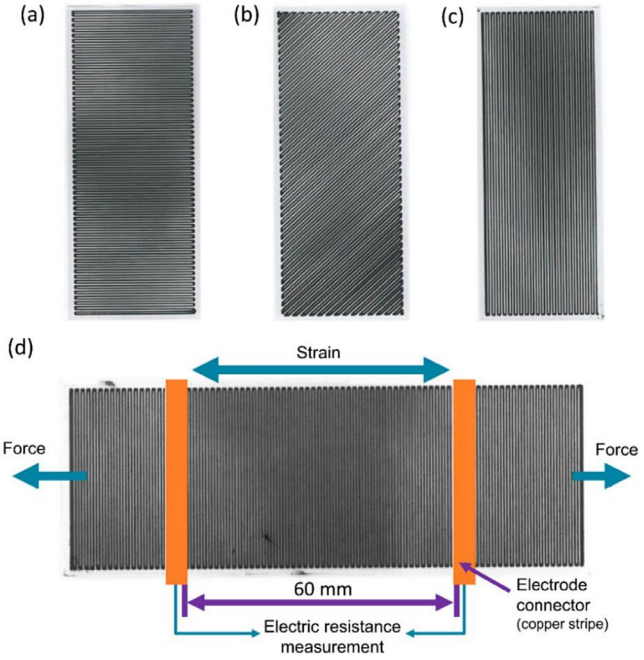

FIGURE 1 | 3D-printed tensile test specimen (120×45 mm) with 40% electrode infill density and different electrode printing directions: (a) 90°, (b) 45°, and (c) 0°. (d) Tensile test specimen (120×45 mm) within the stress-electrical resistance-strain measurement setup. [Color figure can be viewed at wileyonlinelibrary.com]

MX840B" universal measuring amplifier (Hottinger Baldwin Messtechnik, Darmstadt, Germany), with additional circuitry to extend the measuring range up to 80 MΩ. The strain was calculated using the crosshead displacement data from the tensile testing machine and the clamping length.

3 | Results and Discussion

3.1 | Design of the DEA Demonstrators

In this study, a unimorph bending beam actuator (Figure 2a) was used as a demonstrator, which undergoes displacements perpendicular to the plane of the actuator once an external electrical field is applied. For creating stacked actuators, the unimorph elements can be connected in series, and each unimorph element in the structure contributes then to the vertical displacement of the DEA [41]. To obtain the electrically driven movement, the actuator was comprised of two different parts [10]. A passive component, which is non-deformable and was composed of FFF printed NinjaFlex TPU layers, and the active one (dielectric membrane sandwiched between two FFF 3D printed electrodes) which undergoes a defined deformation upon the application of the external electrical field (Figure 2b). It should be noted that the electrode was present on both the active as well as the passive component and consisted of a connecting area, located on the non-deformable section (section 1 in Figure 2b), and an actuation area, located on the deformable section (section 2 in Figure 2b). The connecting area linked the DEA to the external high voltage source and acted as the wiring to the actuation area. The design of section 1 was kept constant for all DEA demonstrators under investigation and was printed with 100% infill density in order to achieve maximum electrical

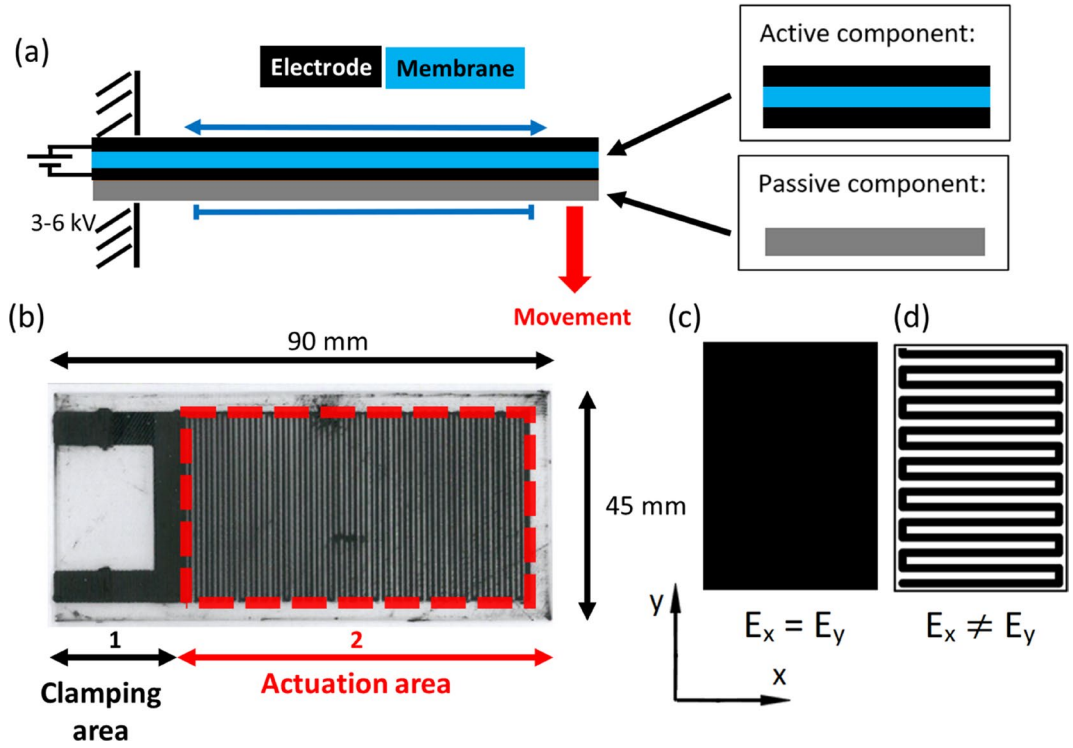

FIGURE 2 | (a) Schematic illustration of the deformation mechanism of a unimorph bending beam actuator composed of an active and passive component upon electrical actuation. (b) Fully 3D-printed actuator with the non-deformable clamping (1) and the deformable actuation section (2). The area of the electrode optimized in the present study is highlighted in red. The Schematic respresentation of two different electrode designs: (c) with 100% infill and quasi isotropic mechanical behavior and (d) with reduced infill and mechanical anisotropy. E_x and E_y represent the Young's moduli in the two perpendicular directions. [Color figure can be viewed at wileyonlinelibrary.com]

conductivity. The schematic of the experimental set-up for characterizing the DEA's endpoint movement and the connection of the DEA to the power supply are provided in Figure S1.

In this study, the electrode geometry of the active component was optimized by varying electrode printing direction and electrode infill density as it is illustrated in Figure 2c. For the initial electrode geometry, the one from our previous work was taken [16]. The electrode infill density was varied, while the electrode printing direction was kept constant at 90°. The electrode infill density variation was directly conducted with the slicing software "Ultimaker Cura 4.6.2". For the electrode infill density, five configurations were used in total. The lowest electrode infill density was 20%, which resulted in a space of 1.6 mm between two adjacently printed electrode lines. For the other electrode infill densities, the corresponding distances were: 27% (1.1 mm), 40% (0.6 mm), 60% (0.27 mm), and 100% (0 mm). The infill density of 100% represents the full electrode with no space between adjacent electrode lines. For each condition, three DEAs were manufactured and investigated.

3.2 | Mechanical and Electrical Properties

For fabricating a DEA, which is able to undergo large deformations, the electrode has to be highly electrically conductive, as compliant as possible in the activation direction, while in the perpendicular direction, a certain rigidity is needed (for structural integrity). It has to be noted that a reduction of the electrode infill density does not only affect its stiffness but also the available 'wire cross section', and thus its electrical conductivity. Hence, the final electrode design has to be a compromise between mechanical and electrical performance.

In a first step, the mechanical stress and electrical resistance of FFF 3D-printed tensile test specimens were recorded as a function of the infill density with the electrodes' infill printed in 0°, 45°, and 90° direction (Figure 3). It is worth mentioning that during the actuation of the DEA, the entire actuator deforms in bending mode rather than in uniaxial tensile direction. Hence, in practice, the electrodes experience both tensile strain and compression. However, for thin films (such as those examined here), tensile tests are the only reasonable test configuration for quantitative mechanical characterization. Consequently, the tensile properties are also used as an approximation for the compression behavior of the electrodes.

During the experiment, the test specimens were uniaxially deformed up to a strain of 300% to cover the typical working strain of a unimorph bending beam DEA, which commonly does not exceed 15% [23, 42]. As an example, the stress–strain curves of test specimens printed in the 45° direction are provided in Figure S3. For the unimorph bending beam DEA examined in this study, an upper strain value of 10% was calculated with a simple geometrical approximation, considering the actuator thickness and the radius of curvature of an actuator movement. Thus, to better highlight the differences in mechanical and electrical properties at low strain values, the data in Figure 3 are presented within the strain operating window of the targeted FFF printed DEA demonstrators.

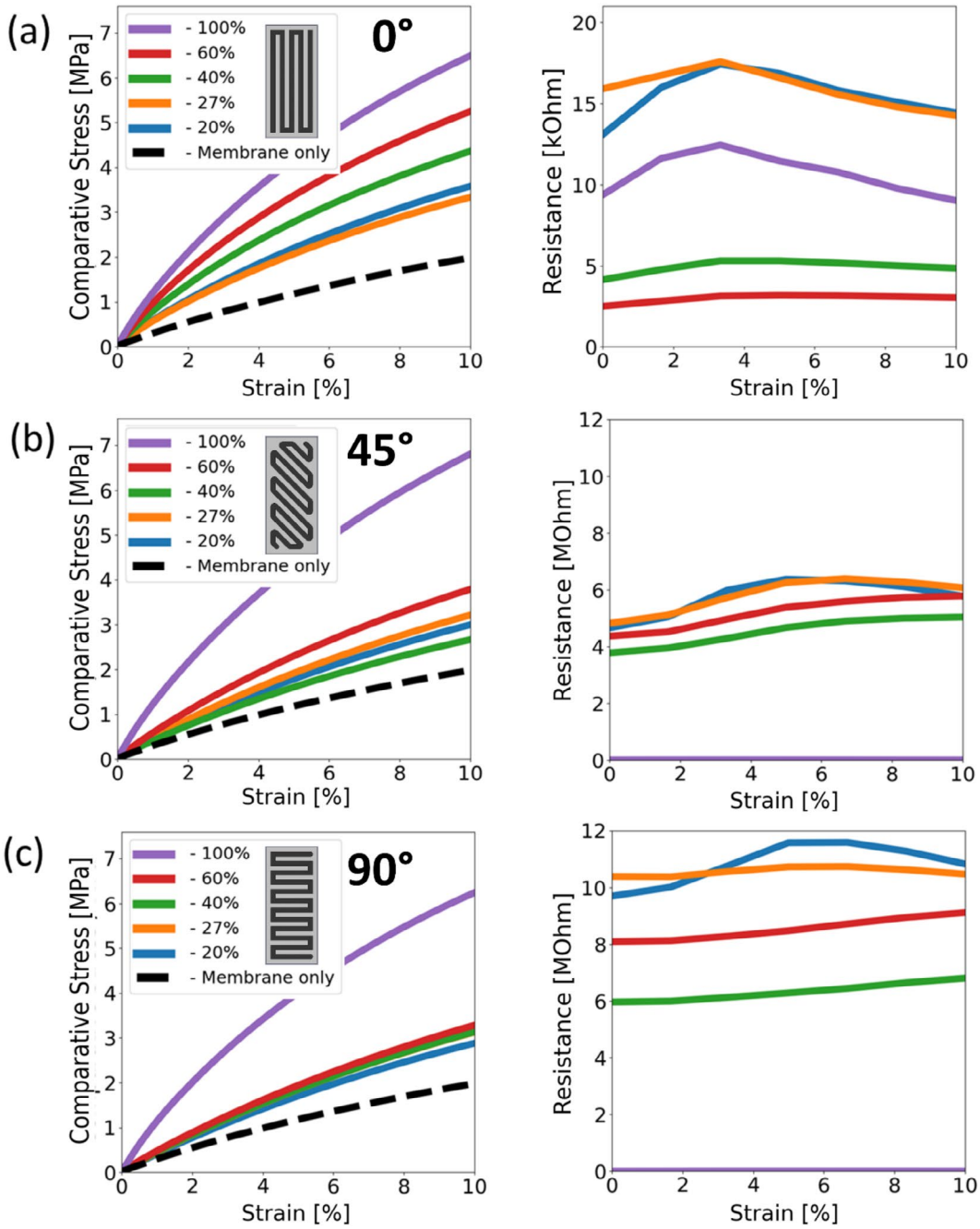

FIGURE 3 | Comparative stress–strain curves and the corresponding electrical resistance-strain plots as a function of the electrode's printing direction and infill density. Printing direction was (a) 0°, (b) 45°, and (c) 90°. It should be noted that the resistance in Figure a is given in kOhm to better highlight the difference in the electrical properties. [Color figure can be viewed at wileyonlinelibrary.com]

The stress values were compared to a reference sample consisting of only one 3D-printed NinjaFlex TPU layer without the electrode. Using a comparative stress, this serves as a benchmark to illustrate the influence of different electrode geometries on the mechanical behavior of the DEA. The comparative stress was calculated by dividing the force values by the cross-sectional area of the reference specimen. It reflects the resistance the DEA's membrane has to overcome during the electrical actuation. The results clearly show that stiffness as well as the comparative stress increase with rising infill density, albeit at a different extents depending on the printing direction. It should be noted that both the geometry of the 3D-printed electrode and the stiffness of the material it is printed of affect the mechanical properties of the final DEA. At low infill densities, the printed electrode follows a meander-like structure, which contributes to its stretchability and compliance [43]. Hence, in the 90° printing direction of the infill, the stress–strain curves do not vary significantly when increasing the infill density from 20% to 60% (Figure 3c). Here, the higher stiffness of the electrically conductive Eel TPU can be compensated by the meander-shaped electrode. The opposite behavior is observed for samples in which the electrode's infill was printed in the 0° direction (Figure 3a).

In this geometry, the mechanical properties are not governed by the meander shape (as it is orthogonal to the measurement direction of the electrode) but mainly by its material properties (Eel TPU is stiffer than NinjaFlex). Thus, a gradual increase in stiffness is observed with increasing filling degree. For the 45° printing direction, geometry as well as material properties are expected to influence the stiffness of the DEA (Figure 3b). Interestingly, the stress values are significantly lower than the ones observed for samples with electrodes printed in the 0° direction. In addition, infill densities between 20% and 40% yield comparable stress–strain values indicating a higher contribution of the geometry of the printed electrodes in the 45° printed samples.

Along with the mechanical properties, the geometry of the electrode significantly affects the electrical performance. Figure S4 presents R/R_0—strain diagrams. These diagrams are derived from the resistance—strain data shown in Figure 3 and demonstrate that the electrical resistance is almost independent of the applied strain within the relevant operational strain range of the DEA ($\leq 10\%$). This is beneficial for both performance and actuation of a DEA, especially when a cyclic actuation is applied [44]. However, it is disadvantageous when it comes to the design of a possible actuator feedback loop for sensing purposes [45]. It should be mentioned here that for higher strains the electrical resistance becomes significantly strain-dependent if the applied strain exceeds 50% (Figure S3) independent of the infill density and printing direction. In general, the resistance-strain values are comparable to the ones reported for electrically conductive rubbers [46]. To facilitate comparison with other studies, the resistance ranges shown in the resistance–strain diagrams (Figure 3) were recalculated into electrical conductivity, taking into account the electrode geometry ($63 \times 37 \times 0.1$ mm) indicated in Figure 2b by red lines. A resistance range of 3–17 kΩ corresponds to a conductivity range of $5.7 - 1\,S \cdot m^{-1}$, while a resistance range of 4–12 MΩ corresponds to a conductivity range of $4.3 - 1.4 \times 10^{-3}\,S \cdot m^{-1}$.The printed electrodes with infill densities ranging between 20% and 60% exhibited an electrical resistance which was 2–3 orders of magnitude higher (independent on the printing direction) than sample printed with an electrode infill density of 100%. By comparing the resistance values of the lower filled electrodes, it has to be considered that the variation in the electrode's infill printing direction is related to a decrease in 'wire length' with decreasing angle of the printing direction. For the 0° printing direction, there is a direct connection between the copper stripes through the electrode 'wires' while for the 90° direction, there is only a connection at the front ends of the meander-like electrode pattern. This explains the relatively high resistance observed in 90° printing direction for 40% and 60% electrode infill densities. Owing to the increased effective 'wire length' of the meander-like pattern, the 60% electrode infill density exhibits a higher resistance than the less dense 40% counterpart. The electrode infill printing direction of 45° lies between the other two in terms of the 'wire length' as well as the electrical resistance. Interestingly, for these samples, the electrical resistance is not significantly affected by the electrode infill density, which indicates that the printing direction plays a key role in the electrode's electrical performance. In contrast, the influence of the infill density becomes more pronounced for the 90° and 0° infill direction.

To complement the experimental approach, a basic electric simulation was conducted to provide additional insights into the electric field distribution of the dielectric membrane. The simulation results showed the highest electric field intensity of 33.33 kV/mm between the upper and lower electrodes (marked red in Figure 4). Since the dielectric membrane thickness was 0.15 mm and the simulated voltage was 5 kV, this result was consistent with the calculated theoretical value (5 kV/0.15 mm = 33.33 kV/mm). However, the more valuable data is the electric field distribution between the adjacent electrodes. For the simulated electrode infill density of 60%, the electric field intensity dropped to

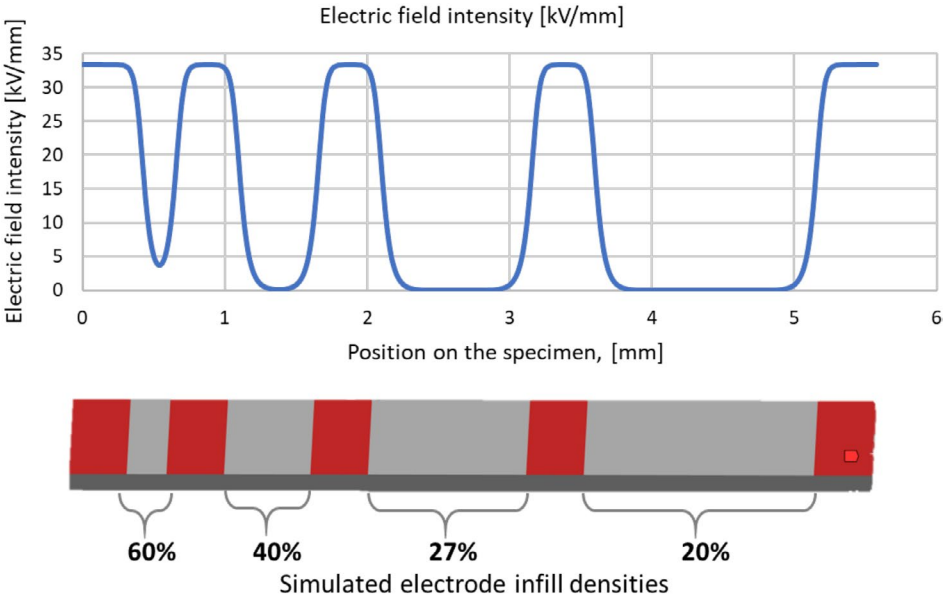

FIGURE 4 | Simulated electric field distribution of a DEA containing electrodes with varying infill densities. [Color figure can be viewed at wileyonlinelibrary.com]

about 4 kV/mm. At a simulated electrode infill density of 40%, the electric field intensity decreased to 0.13 kV/mm. Although this value amounts to only 0.4% of the nominal value (33.33 kV/mm), it provides the optimal geometry among the simulated infill densities. This is due to the electrode's limited impact on the component stiffness (especially for the 90° printing direction as illustrated in Figure 3c) while maintaining a high average electric field, leading to optimal performance. In contrast, the electric field practically vanishes for the two electrode infill densities of 27% and 20%, which makes them not applicable for use in DEAs.

3.3 | Performance of Multi-Material FFF 3D Printed DEA Demonstrators

Based on the resistance–strain data and the electrical field distribution simulations, an electrode characterized by an electrode infill density of 40% and a direction of 90° was chosen for the multi-material FFF printing of the DEA demonstrator. Although the electrode infill direction of 45° resulted in slightly lower comparative stress, the 90° electrode infill direction was favored for general DEA purposes, particularly when certain movement modes are undesirable [47, 48]. The performance of the DEA was assessed by the total actuator displacement by optically following the point at the end of the actuator's free length. The measurements were conducted at an actuation voltage of 4.4 kV, a value chosen based on pretests that confirmed all actuators could withstand this voltage without electrical breakdown. Figure 5a shows the trajectory of the respective actuator undergoing a displacement of 61 mm.

As the optimization target in this study was total displacement, the actuation force was not measured. However, our previous study reported that the blocked force of DEAs with this geometry lies in the range of 1–10 mN. Since the identical electrode material was used, similar response times of approximately 20 s were observed. This is caused by the electrode's higher resistance, which leads to longer charging-actuation times [16].

To verify the assumption that this is the optimal infill density, additional demonstrators with infill densities varying between 20% and 100% were FFF printed.

Figure 5b exhibits the dependence of the total displacement on the electrode infill. The lowest total displacement at 100% electrode infill density can be explained by the fact that this electrode has the highest stiffness and therefore poses the highest resistance against displacement. As the electrode infill density decreases, the total displacement increases, reaching its maximum at 40% infill. The lower the infill density, the more compliant the electrodes become and the lower the resistance of the actuator against the displacement due to the Coulomb effect. A further reduction of the electrode infill density continues to lower the stiffness of the entire DEA system, but the electric field density becomes significantly weaker, leading to a substantial decrease in DEA performance. Thus, in the current set-up, an optimum electrode infill density of 40% exhibited the best

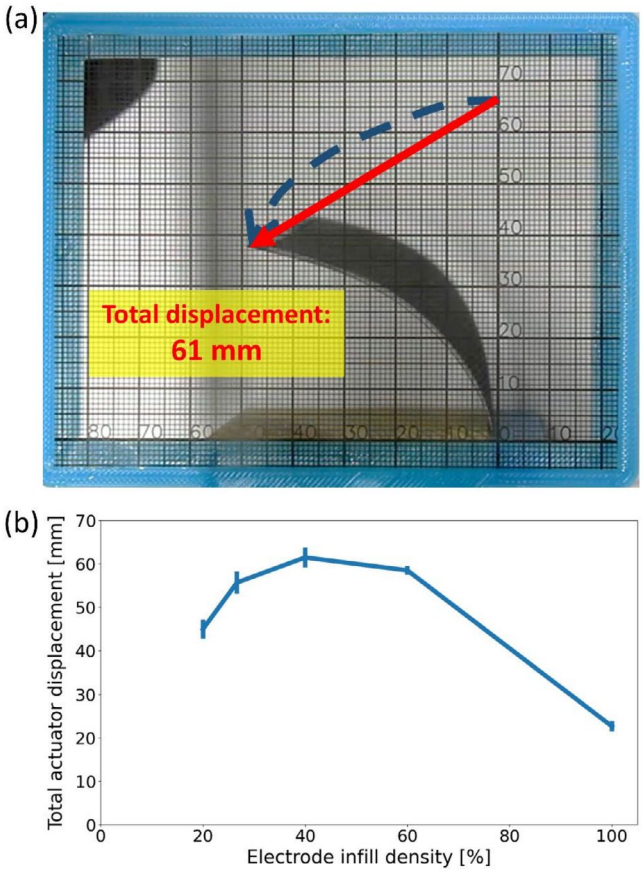

FIGURE 5 | (a) Monitoring the FFF printed DEA displacement by applying 4.4 kV. The dark blue line shows the movement trajectory of the actuator's observed point. (b) Total actuator displacement vs. electrode infill density. Error bars represent the maximum deviation observed among the three 3D printed DEAs for each configuration. [Color figure can be viewed at wileyonlinelibrary.com]

performance, corresponding to about 91% of the actuator's free length.

This is a significant improvement over the maximum actuator displacement of 42% achieved in our previous work [16] and comparable to actuators that have been prepared by conventional techniques or that have not been fully additively manufactured [3, 49–51].

4 | Conclusions

This study comprehensively examined the effect of electrode geometry on the mechanical and electrical behavior of multi-material FFF 3D printed unimorph bending beam DEA. For this, films with varying electrode infill density and electrode infill orientation were prepared, and the stress–strain behavior and the strain-dependent electrical resistance were determined. It was found that infill densities under investigation (20%–60%) affect the mechanical performance of the electrodes in a different manner depending on the printing direction. In 45° and 90° printing directions, they do not play a significant role, while they become relevant by printing samples in the 0° direction. This is mainly related to the meander-like structure of the printed electrodes,

which favors stretchability by design. While positive for the mechanical DEA performance, this meander-like structure of the electrode negatively influences the electrical DEA performance because of an increased wire length and thus electrical resistance.

In a second step, the maximum displacement of fully 3D printed DEA demonstrators was studied at a 90° infill direction with varying infill densities. The results clearly show that the displacement is affected by both mechanical stiffness and electrical properties (i.e., electrical field intensity and resistance). While the lowest electrical resistance was obtained by a fully printed electrode (100% infill density), the resulting displacement was less pronounced as the electrode compromised on the total compliance of the DEA. The best performance was obtained with a 40% electrode infill density, which resulted in the maximum actuator displacement of 91% relative to its free length. The data were also in good agreement with the tensile properties and simulated electrical field distributions.

While the optimization of the electrode's geometric parameters in the chosen set-up is limited, follow-up studies will be dedicated to the optimization of the electrode material properties. The development of a more electrically conductive FFF filament has the potential to enable new functionalities, such as sensing and intrinsic heating, which may be implemented into the DEA. In addition, it is expected to pave the way toward a faster dielectric actuator response, which is a highly sought-after property in soft robotic applications.

Author Contributions

Ivan Raguž: conceptualization (supporting), investigation (lead), methodology (lead), visualization (lead), writing – original draft (lead). **Michael Berer:** conceptualization (lead), project administration (lead), supervision (lead), validation (lead), writing – review and editing (supporting). **Clemens Holzer:** resources (supporting), supervision (supporting), validation (supporting), writing – review and editing (supporting). **Bram Vanderborght:** investigation (supporting), methodology (supporting), validation (supporting), writing – review and editing (supporting). **Joost Brancart:** investigation (supporting), methodology (supporting), validation (supporting), writing – review and editing (supporting). **Sandra Schlögl:** funding acquisition (lead), validation (supporting), visualization (supporting), writing – review and editing (lead).

Acknowledgments

The research work of this study was performed in the COMET-Module projects "CHEMITECTURE" (project-no.: 21647048) and "Repairtecture" (project-no.: 904927) at the Polymer Competence Center Leoben GmbH (PCCL, Austria) within the framework of the COMET program of the Federal Ministry for Climate Action, Environment, Energy, Mobility, Innovation, and Technology and the Federal Ministry for Digital and Economic Affairs with contributions by the Department of Polymer Engineering and Science/Montanuniversitaet Leoben; Physical Chemistry and Polymer Science lab, Sustainable Materials Engineering/Vrije Universiteit Brussel and Brubotics at Vrije Universiteit Brussel and imec. The PCCL is funded by the Austrian Government and the State Governments of Styria, Lower Austria, and Upper Austria. The authors acknowledge the Fonds Wetenschappelijk Onderzoek for the senior postdoctoral fellowship of Joost Brancart (12W4719N). Special thanks go to Joamin Gonzalez-Gutierrez for fruitful discussions and to Gerald Meier for performing the work on the tensile testing machine. Open Access funding provided by Montanuniversitat Leoben/KEMÖ.

Conflicts of Interest

The authors declare no conflicts of interest.

Data Availability Statement

The data that support the findings of this study are available from the corresponding author upon reasonable request.

References

1. C. Lee, M. Kim, Y. J. Kim, et al., "Soft Robot Review," *International Journal of Control, Automation and Systems* 15 (2017): 3–15.

2. E. Roels, S. Terryn, F. Iida, et al., "Processing of Self-Healing Polymers for Soft Robotics," *Advanced Materials* 34 (2022): e2104798.

3. O. A. Araromi, I. Gavrilovich, J. Shintake, et al., "Rollable Multisegment Dielectric Elastomer Minimum Energy Structures for a Deployable Microsatellite Gripper," *IEEE/ASME Transactions on Mechatronics* 20 (2015): 438–446.

4. R. Pelrine, P. Sommer-Larsen, R. D. Kornbluh, et al., *Smart Structures and Materials 2001: Electroactive Polymer Actuators and Devices*, ed. Y. Bar-Cohen (SPIE, 2001).

5. A. O'Halloran, F. O'Malley, and P. McHugh, "A Review on Dielectric Elastomer Actuators, Technology, Applications, and Challenges," *Journal of Applied Physics* 104 (2008): 71101.

6. L. J. Romasanta, M. A. Lopez-Manchado, and R. Verdejo, "Increasing the Performance of Dielectric Elastomer Actuators: A Review From the Materials Perspective," *Progress in Polymer Science* 51 (2015): 188–211.

7. Y. Guo, L. Liu, Y. Liu, and J. Leng, "Review of Dielectric Elastomer Actuators and Their Applications in Soft Robots," *Advanced Intelligent Systems* 3 (2021): 2000282.

8. R. Pelrine, R. Kornbluh, J. Joseph, R. Heydt, and S. Chiba, "High-Field Deformation of Elastomeric Dielectrics for Actuators," *Materials Science & Engineering, C: Materials for Biological Applications* 11 (2000): 89–100.

9. J.-S. Plante and S. Dubowsky, "Large-Scale Failure Modes of Dielectric Elastomer Actuators," *International Journal of Solids and Structures* 43 (2006): 7727–7751.

10. R. Kornbluh, *Dielectric Elastomers as Electromechanical Transducers: Fundamentals, Materials, Devices, Models and Applications of an Emerging Electroactive Polymer Technology*, ed. F. Carpi (Elsevier, 2008), 79–90.

11. X. Zhao and Z. Suo, "Electrostriction in Elastic Dielectrics Undergoing Large Deformation," *Journal of Applied Physics* 104 (2008): 123530.

12. G. Kofod, P. Sommer-Larsen, R. Kornbluh, and R. Pelrine, "Actuation Response of Polyacrylate Dielectric Elastomers," *Journal of Intelligent Material Systems and Structures* 14 (2003): 787–793.

13. E. I. Zyrianova, S. V. Pak, V. A. Demina, et al., "Polyurethane-Based Composite Materials Promising for Dielectric Actuators," *Nanotechnologies in Russia* 19 (2024): 937–948.

14. J. Kim, J. W. Kim, H. C. Kim, L. Zhai, H.-U. Ko, and R. M. Muthoka, "Review of Soft Actuator Materials," *International Journal of Precision Engineering and Manufacturing* 20 (2019): 2221–2241.

15. R. Pelrine, R. Kornbluh, and G. Kofod, "High-Strain Actuator Materials Based on Dielectric Elastomers," *Advanced Materials* 12 (2000): 1223–1225.

16. I. Raguž, M. Berer, M. Fleisch, et al., "Soft Dielectric Actuator Produced by Multi-Material Fused Filament Fabrication 3D Printing," *Polymers for Advanced Techs* 34: (2023): 1967–1978.

17. D. Gonzalez, J. Garcia, and B. Newell, "Electromechanical Characterization of a 3D Printed Dielectric Material for Dielectric Electroactive Polymer Actuators," *Sensors and Actuators A: Physical* 297 (2019): 111565.

18. A. Wiranata, Y. Ishii, N. Hosoya, and S. Maeda, "Simple and Reliable Fabrication Method for Polydimethylsiloxane Dielectric Elastomer Actuators Using Carbon Nanotube Powder Electrodes," *Advanced Engineering Materials* 23 (2021): 2001181.

19. K. Bertoldi, V. Vitelli, J. Christensen, and M. van Hecke, "Flexible Mechanical Metamaterials," *Nature Reviews Materials* 2 (2017): 17066.

20. A. Nicolau-Kuklińska, P. Latko-Durałek, P. Nakonieczna, K. Dydek, A. Boczkowska, and J. Grygorczuk, "A New Electroactive Polymer Based on Carbon Nanotubes and Carbon Grease as Compliant Electrodes for Electroactive Actuators," *Journal of Intelligent Material Systems and Structures* 29 (2018): 1520–1530.

21. S. Sikulskyi, S. L. Yu, E. A. Rojas-Nastrucci, J. Park, and D. Kim, *Electroactive Polymer Actuators and Devices (EAPAD) XXII*, ed. Y. Bar-Cohen, I. A. Anderson, and H. R. Shea (SPIE, 2020).

22. S. Schlatter, S. Rosset, and H. Shea, *Electroactive Polymer Actuators and Devices (EAPAD) 2017*, ed. Y. Bar-Cohen (SPIE, 2017).

23. R. E. Pelrine, R. D. Kornbluh, and J. P. Joseph, "Electrostriction of Polymer Dielectrics With Compliant Electrodes as a Means of Actuation," *Sensors and Actuators A: Physical* 64 (1998): 77–85.

24. M. R. O'Neill, E. Acome, S. Bakarich, et al., "Rapid 3D Printing of Electrohydraulic (HASEL) Tentacle Actuators," *Advanced Functional Materials* 30 (2020): 2005244.

25. W. Zhang, J. Ma, W. Zhang, et al., "A Multidimensional Nanostructural Design Towards Electrochemically Stable and Mechanically Strong Hydrogel Electrodes," *Nanoscale* 12 (2020): 6637–6643.

26. H. Wu, W. P. Fahy, S. Kim, et al., "Recent Developments in Polymers/Polymer Nanocomposites for Additive Manufacturing," *Progress in Materials Science* 111 (2020): 100638.

27. Z. Li, M. Sheng, M. Wang, P. Dong, B. Li, and H. Chen, "Stacked Dielectric Elastomer Actuator (SDEA): Casting Process, Modeling and Active Vibration Isolation," *Smart Materials and Structures* 27 (2018): 75023.

28. C. R. Kelley and J. L. Kauffman, "Towards Wearable Tremor Suppression Using Dielectric Elastomer Stack Actuators," *Smart Materials and Structures* 30 (2021): 25006.

29. J. Rossiter, P. Walters, and B. Stoimenov, "Printing 3D dielectric elastomer actuators for soft robotics," in *Electroactive Polymer Actuators and Devices (EAPAD)*, vol. 7287-15 (SPIE, 2009), https://doi.org/10.1117/12.815746.

30. S. C. Ligon, R. Liska, J. Stampfl, M. Gurr, and R. Mülhaupt, "Polymers for 3D Printing and Customized Additive Manufacturing," *Chemical Reviews* 117 (2017): 10212–10290.

31. U. Shaukat, E. Rossegger, and S. Schlögl, "A Review of Multi-Material 3D Printing of Functional Materials via Vat Photopolymerization," *Polymers* 14 (2022): 2449.

32. M. Spoerk, C. Savandaiah, F. Arbeiter, et al., "Anisotropic Properties of Oriented Short Carbon Fibre Filled Polypropylene Parts Fabricated by Extrusion-Based Additive Manufacturing," *Composites Part A: Applied Science and Manufacturing* 113 (2018): 95–104.

33. M. Spoerk, C. Holzer, and J. Gonzalez-Gutierrez, "Material Extrusion-Based Additive Manufacturing of Polypropylene: A Review on How to Improve Dimensional Inaccuracy and Warpage," *Journal of Applied Polymer Science* 137 (2020): 48545.

34. S. Cano, T. Lube, P. Huber, et al., "Influence of the Infill Orientation on the Properties of Zirconia Parts Produced by Fused Filament Fabrication," *Materials* 13 (2020): 3158.

35. H. M. Lee, J. Sung, B. Ko, et al., "Modeling and Application of Anisotropic Hyperelasticity of PDMS Polymers With Surface Patterns Obtained by Additive Manufacturing Technology," *Journal of the Mechanical Behavior of Biomedical Materials* 118 (2021): 104412.

36. T. B. Palmić and J. Slavič, "Single-Process 3D-Printed Stacked Dielectric Actuator," *International Journal of Mechanical Sciences* 230 (2022): 107555.

37. NinjaTek, "NinjaTek NinjaFlex TPU Filament."

38. Fenner Inc., "Filament Eel TPU 3D," 2016.

39. M. Huang, Y. Zhang, L. Liu, and J. Wang, "Effects of Insulation Structure on Electric Field Distribution of Valve-Side Outlet Device of Converter Transformer," *IOP Conference Series: Materials Science and Engineering* 452 (2018): 32071.

40. S. Y. Shevchenko, D. O. Danylchenko, A. E. Potryvay, S. I. Dryvetsky, and V. M. Tsyupa, "Bulletin of the National Technical University "KhPI"," *Series: Energy: Reliability & Energy Efficiency* (2022): 79–85.

41. Q.-M. Wang and L. E. Cross, "Performance Analysis of Piezoelectric Cantilever Bending Actuators," *Ferroelectrics* 215 (1998): 187–213.

42. O. A. Araromi and S. C. Burgess, "A Finite Element Approach for Modelling Multilayer Unimorph Dielectric Elastomer Actuators with Inhomogeneous Layer Geometry," *Smart Materials and Structures* 21 (2012): 32001.

43. S. Biswas, J. Reiprich, J. Pezoldt, M. Hein, T. Stauden, and H. O. Jacobs, "Stress-Adaptive Meander Track for Stretchable Electronics," *Flexible and Printed Electronics* 3 (2018): 32001.

44. C. Tang, B. Du, S. Jiang, Z. Wang, X.-J. Liu, and H. Zhao, "A Review on High-Frequency Dielectric Elastomer Actuators: Materials, Dynamics, and Applications," *Advanced Intelligent Systems* 6 (2024): 2300047.

45. A. Poulin and S. Rosset, "An Open-Loop Control Scheme to Increase the Speed and Reduce the Viscoelastic Drift of Dielectric Elastomer Actuators," *Extreme Mechanics Letters* 27 (2019): 20–26.

46. S. Rosset and H. R. Shea, "Flexible and Stretchable Electrodes for Dielectric Elastomer Actuators," *Applied Physics A* 110 (2013): 281–307.

47. B. O'Brien, E. Calius, S. Xie, and I. Anderson, *Electroactive Polymer Actuators and Devices (EAPAD) 2008*, ed. Y. Bar-Cohen (SPIE, 2008).

48. H. Zhao, A. Hussain, A. Israr, et al., "Robotics," 7 (2020).

49. B. O'Brien, T. McKay, E. Calius, S. Xie, and I. Anderson, "Finite Element Modelling of Dielectric Elastomer Minimum Energy Structures," *Applied Physics A* 94 (2009): 507–514.

50. K.-R. Heng, A. S. Ahmed, M. Shrestha, and G.-K. Lau, *Electroactive Polymer Actuators and Devices (EAPAD) 2017*, ed. Y. Bar-Cohen (SPIE, 2017).

51. F. Zhou, M. Zhang, X. Cao, et al., "Fabrication and Modeling of Dielectric Elastomer Soft Actuator With 3D Printed Thermoplastic Frame," *Sensors and Actuators A: Physical* 292 (2019): 112–120.

Supporting Information

Additional supporting information can be found online in the Supporting Information section. **Data S1:** Supporting Information.